JMEPEG (2014) 23:3875–3886
DOI: 10.1007/s11665-014-1189-z
©The Author(s). This article is published with open access at Springerlink.com
1059-9495/$19.00

Sintering Behavior and Mechanical Properties of NiAl, Al_2O_3, and NiAl-Al_2O_3 Composites

M. Chmielewski, S. Nosewicz, K. Pietrzak, J. Rojek, A. Strojny-Nędza, S. Mackiewicz, and J. Dutkiewicz

(Submitted April 28, 2014; in revised form July 12, 2014; published online August 12, 2014)

It is commonly known that the properties of sintered materials are strongly related to technological conditions of the densification process. This paper shows the sintering behavior of a NiAl-Al_2O_3 composite, and its individual components sintered separately. Each kind of material was processed via the powder metallurgy route (hot pressing). The progress of sintering at different stages of the process was tested. Changes in the microstructure were examined using scanning and transmission electron microscopy. Metal-ceramics interface was clean and no additional phases were detected. Correlation between the microstructure, density, and mechanical properties of the sintered materials was analyzed. The values of elastic constants of NiAl/Al_2O_3 were close to intermetallic ones due to the volume content of the NiAl phase particularly at low densities, where small alumina particles had no impact on the composite's stiffness. The influence of the external pressure of 30 MPa seemed crucial for obtaining satisfactory stiffness for three kinds of the studied materials which were characterized by a high dense microstructure with a low number of isolated spherical pores.

Keywords ceramics, composites, electron, intermetallic, metallic matrix, microscopy, powder metallurgy, sintering, structural

1. Introduction

Sintering is a complex thermally activated physicochemical process which takes place at an increased temperature (Ref 1). A great number of factors linked to both the technological process conditions and physical characteristics of source materials exert an influence on sintering. The predominant parameters of technological nature include the temperature, time, heating and cooling speed, pressure, and atmosphere (Ref 2, 3). Determining the relation between the process conditions as well as the structure and properties of single-phase materials does not constitute a problem. This correlation is much more complex in case of multiphase materials such as ceramics-metal composite materials. The properties of metals and ceramic materials are very diverse because of their structure. Difficulties in coupling these materials result from their dissimilar atomic bonds, non-wettability of ceramic materials by liquid metals or generation of high thermal stress while cooling caused by differences in their mechanical and thermal properties (Ref 4-9). A good example of such diphase materials is composites with a NiAl matrix reinforced by the ceramic phase in the form of Al_2O_3 particles.

Intermetallic compound NiAl is a promising material for high temperature applications, particularly suitable as a bond coat in thermal barrier coatings (TBCs) (Ref 10). Ni-Al intermetallic phases belong to the group of modern constructional materials of low density and with advantageous properties. They are characterized e.g., by a high melting temperature, high resistance to oxidation at high temperatures (to about 1200 °C), high value of the Young's modulus, stability in an increased temperature, high mechanical, fatigue, tensile and compressive strengths (also at high temperatures), and good frictional wear resistance (Ref 11-14). This unparalleled combination of unique physicochemical and mechanical properties offers a wide range of application possibilities for these materials. They are widely used in technologically developed countries in the automobile, aircraft, spacecraft, metallurgical, chemical, and power generation industries. However, intermetallic compounds also manifest drawbacks, i.e., they are quite brittle at room temperature (RT) which makes their mechanical processing very difficult and restricts their application range. These drawbacks can be obviated by modifying material's chemical composition. The authors of (Ref 15) report that non-reactive particles improve the properties of the NiAl matrix as a result of changing the fracture mode from intergranular to transgranular in accordance with Cook-Gordon mechanism (Ref 16). In (Ref 17) the author indicates plastic deformation as an additional factor in the toughening process.

One of the most interesting and, at the same time, one of the most complex problems in relation to composite materials is the determination of relation between the structure of the matrix/

M. Chmielewski and **A. Strojny-Nędza**, Institute of Electronic Materials Technology, Wolczynska 133, 01-919 Warsaw, Poland; **S. Nosewicz, J. Rojek,** and **S. Mackiewicz**, Institute of Fundamental Technological Research, Polish Academy of Sciences, Pawinskiego 5B, 02-106 Warsaw, Poland; **K. Pietrzak**, Institute of Electronic Materials Technology, Wolczynska 133, 01-919 Warsaw, Poland and Institute of Fundamental Technological Research, Polish Academy of Sciences, Pawinskiego 5B, 02-106 Warsaw, Poland; and **J. Dutkiewicz**, Institute of Metallurgy and Materials Science, Reymonta 25, 30-058 Cracow, Poland. Contact e-mails: marcin.chmielewski@itme.edu.pl, snosew@ippt.pan.pl, katarzyna.pietrzak@itme.edu.pl, jrojek@ippt.pan.pl, agata.strojny@itme.edu.pl, smackiew@ippt.pan.pl, and j.dutkiewicz@imim.pl.

reinforcement interface and the properties of composites. For ceramics-metal composite materials, various coupling types of these two phases are possible, i.e., mechanical coupling, coupling as a result of rewetting, and the partial formation of solid solutions, as well as the formation of a compound resulting from the reaction at the boundary of the components. Formation mechanism determines the quality of all enumerated couplings and, at the same time, the properties of the composite which means that coupling can be mechanical, adhesive, diffusive, or reactive. Each of these couplings is characterized by a different formation mechanism, quality as well as durability linked to interaction between the composite's components. The authors of (Ref 18) examined the quality of coupling at the NiAl-Al_2O_3 boundary and found it to be the weakest area in the composite, where cracks were likely to appear and be propagated. An optimized bond coat in case of NiAl-Al_2O_3 contains various additives such as Co, Cr or Pt, and reactive elements (REs) such as Y, Hf, or Dy (Ref 10, 28).

In the present work, the impact of technological parameters of the sintering process on the microstructure of the NiAl-Al_2O_3 composite was analyzed with the main focus on the metal-ceramics interface. In addition, both the sintering kinetics of separately sintered composite components and the changes in the mechanical properties of materials observed during successive sintering phases were determined.

The results presented in this paper constitute an integral part of a broader research programme focused on the manufacture of NiAl-based composite materials. These works are aimed at elaborating technological conditions enabling obtaining composites with target properties. The resultant material is planned to be used in internal combustion engines as valve seats. At present, applicability tests are being performed under conditions resembling true engine load in order to verify the suitability of the developed materials.

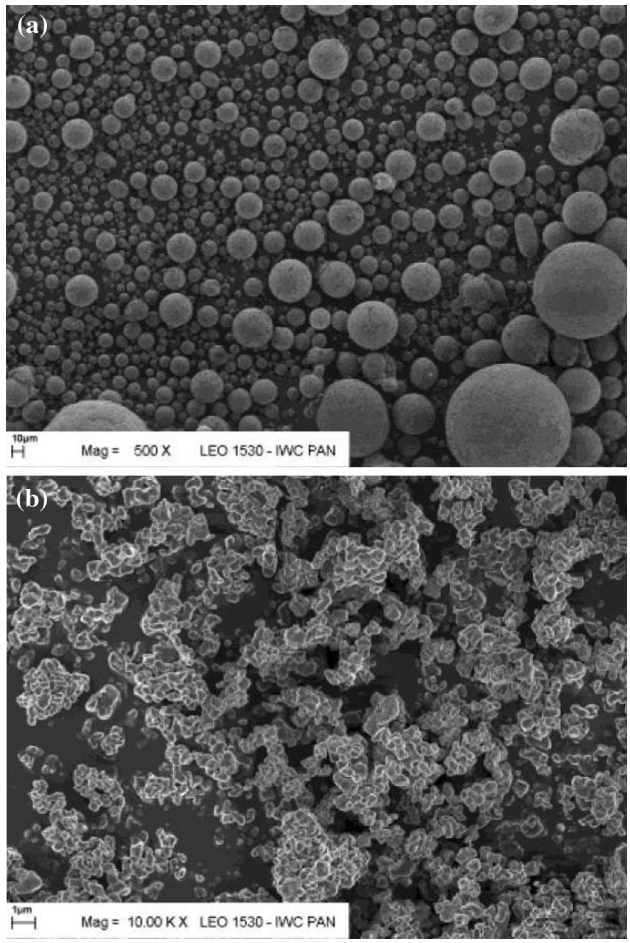

Fig. 1 SEM imaging of starting materials: (a) NiAl, (b) Al_2O_3

2. Experimental Procedure

Commercially available NiAl powders (Fig. 1a, by Goodfellow) and aluminum oxide powders (Fig. 1b, by NewMet Koch) were used in the present work.

Research tasks included the characterization of the grain size distribution of the output powders performed using the Clemex image analysis system. The particle size distribution was analyzed as a function of Feret's diameter (d). As a result, the average Feret's diameter (d_A) was calculated. Based on the analysis, the average size of the NiAl particles was found to be d_{NiAl} = 9.71 µm (the size range is from 1 to almost 100 µm) and that of the Al_2O_3 particles d_{Al2O3} = 2.28 µm (from 0.2 to 5 µm).

Technological sintering trials were carried out for pure NiAl, pure Al_2O_3 as well as for the mixtures of these powders with the following volume fraction: 80%NiAl/20%Al_2O_3.

This composition was selected following the theoretical studies of the mechanical properties of the components of composite materials, taking into consideration their possible application in an internal combustion engine as a valve seat. The mixing test was carried out in a Pulverisette 6 planetary mill with a 250 ml container in air atmosphere. Both the lining of the container and milling balls (Ø10 mm in diameter) were made of tungsten carbide doped with cobalt. Mixing process parameters were experimentally selected based on previous works of the authors (Ref 19, 20). An even distribution of aluminum oxide in the mixture was obtained under the following conditions: rotational speed ω = 100 rpm, BPR coefficient 5:1, and time of 1 h.

All materials were pressure-sintered in the ASTRO HP50-7010 press using hot-pressing in a graphite cylindrical die with a diameter of 13 mm in an argon protective atmosphere. A variety of technological conditions were used to describe the sintering kinetics of both individual components (NiAl, Al_2O_3) and the two-phase material. The parameters of sintering were as follows:

- sintering temperature T_s—1300, 1350 and 1400 °C,
- sintering time t_s—0, 10 and 30 min,
- pressure p—5 and 30 MPa.

Temperature was increased from the RT to the sintering temperature T_s with the heating rate of 15 °C/min for all examined materials. The samples were kept at T_s during the interval (sintering time) t_s and naturally cooled down to the RT. In case of t_s = 0 min sintering time, the samples were heated to the sintering temperature and immediately cooled down. The pressure was applied from the beginning of the sintering process to the end of the thermal cycle.

Microstructural investigations included the analyses using scanning electron microscopy (SEM, Hitachi S4100) and transmission microscopy (TEM, Tedmai G2). The samples were mechanically cut using a diamond saw, then grinded and

polished. For the purpose of SEM observations, they were covered with a thin layer of carbon and for TEM they were additionally thinned using abrasive paper. Thin lamellae were cut using FIB Quanta 200 3D FEI instruments or thinned using a Leica EM RES 101 ion beam thinner.

The examination of NiAl, Al_2O_3, and NiAl-Al_2O_3 composites density was carried out following the hydrostatic method.

To verify the elastic properties of the sintered samples, the measurements based on ultrasonic wave propagation were conducted. Ultrasonic measurements are a common tool used to determine the elastic properties of particulate materials (Ref 21-23). In the present studies, the obtained sintered samples were assumed to be isotropic materials due to random orientation of the grains and distributed in the material's volume. Accordingly, elastic properties were described in terms of two independent elastic constants, the Young's modulus, E, and Poisson's ratio, υ, which can be deduced from the elastic waves theory (Ref 21):

$$E = \rho \frac{(3V_L^2 V_T^2 - 4V_T^4)}{(V_L^2 - V_T^2)}, \quad \text{(Eq 1)}$$

$$\upsilon = \frac{(0.5V_L^2 - V_T^2)}{(V_L^2 - V_T^2)}, \quad \text{(Eq 2)}$$

where ρ—bulk density, V_L—velocity of longitudinal ultrasonic waves, V_T—velocity of shear ultrasonic waves.

For measurements of ultrasonic velocities in the sintered samples, the pulse-echo contact technique was employed. A detailed description of the ultrasonic measurements used in the determination of the elastic constant of the sintered NiAl/Al_2O_3 composite material was introduced by the authors in (Ref 24).

Table 1 Evolution of the bulk and relative density of the hot-pressed Al_2O_3 ceramics sintered in different combinations of sintering temperatures and pressures (Al_2O_3 theoretical density—3.97 g/cm^3)

Temperature/pressure T_S (°C)/p (MPa)	t_S = 0 min		t_S = 10 min		t_S = 30 min	
	ρ (g/cm^3)	ρ_{rel}	ρ (g/cm^3)	ρ_{rel}	ρ (g/cm^3)	ρ_{rel}
1300/5	2.58	0.65	2.77	0.70	3.34	0.84
1350/5	2.93	0.74	3.13	0.79	3.61	0.91
1400/5	3.32	0.84	3.38	0.85	3.82	0.96
1300/30	3.45	0.87	3.58	0.90	3.80	0.96
1350/30	3.56	0.90	3.85	0.97	3.93	0.99
1400/30	3.86	0.97	3.88	0.98	3.97	1.00

Table 2 Evolution of the bulk and relative density of the hot-pressed NiAl intermetallic compounds sintered in different combinations of sintering temperatures and pressures (NiAl theoretical density—5.91 g/cm^3)

Temperature/pressure T_S (°C)/p (MPa)	t_S = 0 min		t_S = 10 min		t_S = 30 min	
	ρ (g/cm^3)	ρ_{rel}	ρ (g/cm^3)	ρ_{rel}	ρ (g/cm^3)	ρ_{rel}
1300/5	4.66	0.79	4.88	0.82	4.90	0.83
1350/5	4.75	0.80	4.97	0.84	5.13	0.87
1400/5	5.24	0.89	5.33	0.90	5.45	0.92
1300/30	5.25	0.89	5.43	0.92	5.52	0.93
1350/30	5.35	0.91	5.52	0.93	5.73	0.97
1400/30	5.42	0.92	5.78	0.98	5.86	0.99

Table 3 Evolution of the bulk and relative density of the hot-pressed NiAl/Al_2O_3 composite sintered in different combinations of sintering temperatures and pressures (NiAl/20%Al_2O_3 theoretical density—5.52 g/cm^3)

Temperature/pressure T_S (°C)/p (MPa)	t_S = 0 min		t_S = 10 min		t_S = 30 min	
	ρ (g/cm^3)	ρ_{rel}	ρ (g/cm^3)	ρ_{rel}	ρ (g/cm^3)	ρ_{rel}
1300/5	3.86	0.70	4.01	0.73	4.10	0.74
1350/5	4.02	0.73	4.16	0.75	4.42	0.80
1400/5	4.11	0.74	4.28	0.78	4.92	0.89
1300/30	4.99	0.90	5.03	0.91	5.44	0.99
1350/30	5.24	0.95	5.35	0.97	5.50	1.00
1400/30	5.27	0.95	5.37	0.97	5.51	1.00

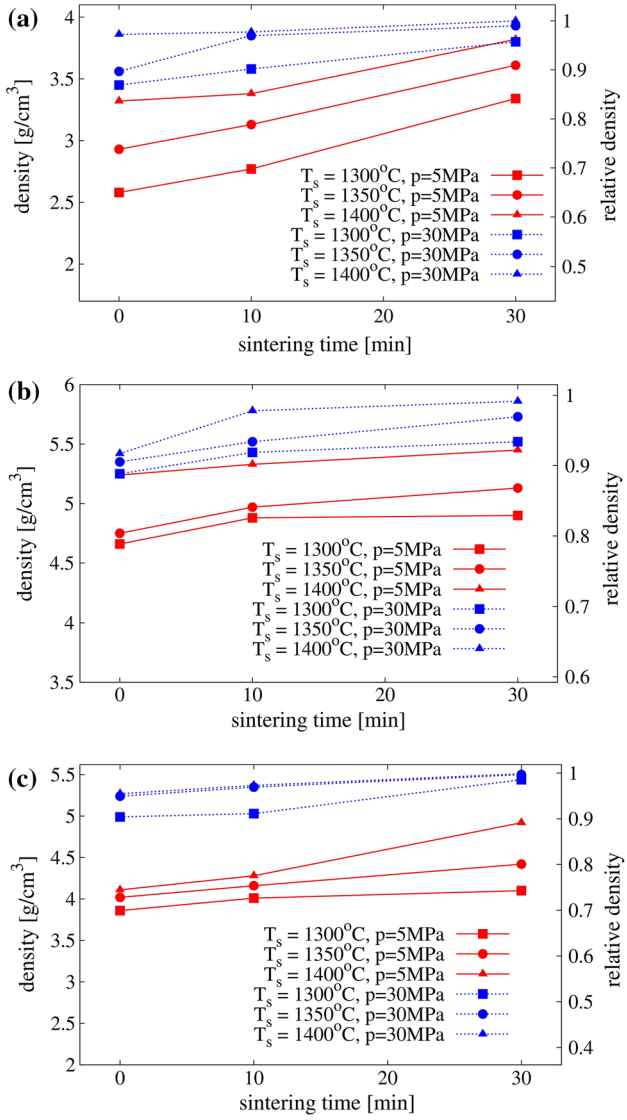

Fig. 2 Density evolution of: (a) pure Al_2O_3, (b) pure NiAl and (c) NiAl/Al_2O_3 composite material sintered under 5 and 30 MPa pressures at sintering temperatures of: 1300, 1350 and 1400 °C

3. Results and Discussion

3.1 Porosity Evaluation

The sintering degree was assessed based on the relative density, ρ_{rel}, defined as the ratio of the measured bulk (apparent) density ρ to the theoretical density ρ_{theo} for the fully dense material (Ref 25, 26):

$$\rho_{rel} = \frac{\rho}{\rho_{theo}}. \quad \text{(Eq 3)}$$

Results of density measurements are provided in Tables 1, 2, 3. Density evolution curves for different combinations of temperature and time parameters are plotted in Fig. 2.

It can be deduced from the observation of density measurements that in the selected range of sintering parameters almost fully dense materials were obtained. All three technological parameters (temperature, time, and pressure) have a significant influence on the degree of the material's densification. The importance of each of them is different but cannot be analyzed separately because only their proper combination is likely to provide the best results in terms of materials densification.

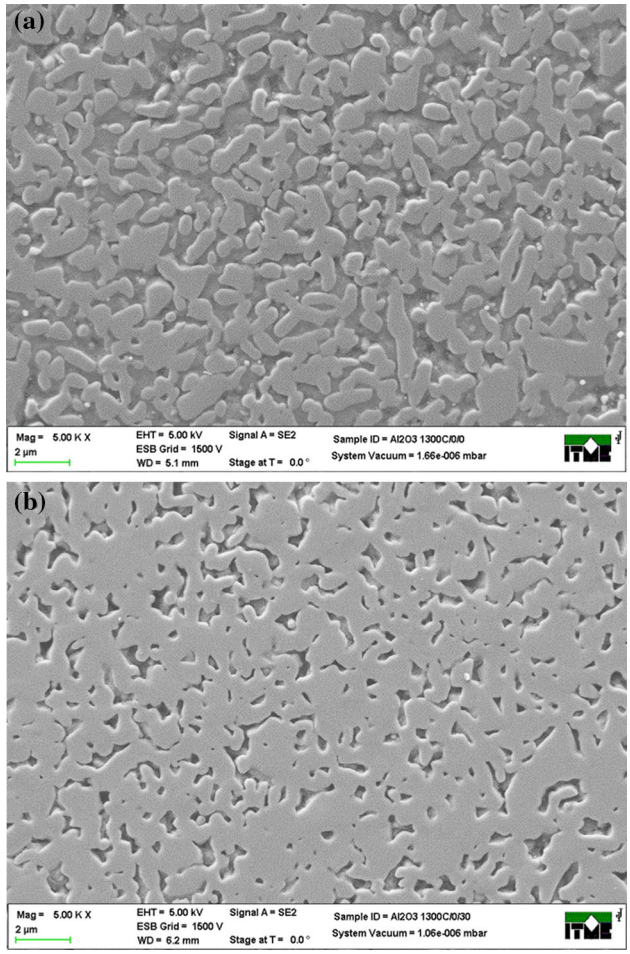

Fig. 3 SEM images of sintered aluminum oxide at different conditions: (a) T_s = 1300 °C, t_s = 0 min, p = 5 MPa, (b) T_s = 1300 °C, t_s = 0 min, p = 30 MPa

As can be seen in Tables 1, 2, 3, the pressure plays a very important role in the sintering process of all three types of materials. Relative densities for single- and two-phase materials were different and the best results were obtained for pure ceramics (almost 96%). An increase of the pressure to the level of 30 MPa results in a much higher degree of densification even at lower temperatures. It is correlated with the easier grain regrouping process at an early stage, the activation of diffusion flow,s and an easier pore elimination at the final stage of sintering.

Sintering is a time-consuming process and it is obvious that when the sintering time is extended, the density of the material should also rise. Figure 2 shows that in all examined cases an increase in the sintering time improved the relative density of materials, for both pressures, i.e., 5 and 30 MPa. The sintering temperature depends on the physical-chemical properties of the sintered powders as well as the grain size and shape. In case of unary systems, it is assumed that the sintering temperature is 0.6-0.8 of a material's melting point. For multiphase materials, the choice of the sintering temperature is more complicated. It is related to the volume fractions of components, their solubility and wettability, and the surface energy connected with the grain size and specific surface area, etc. The mass flow is strictly

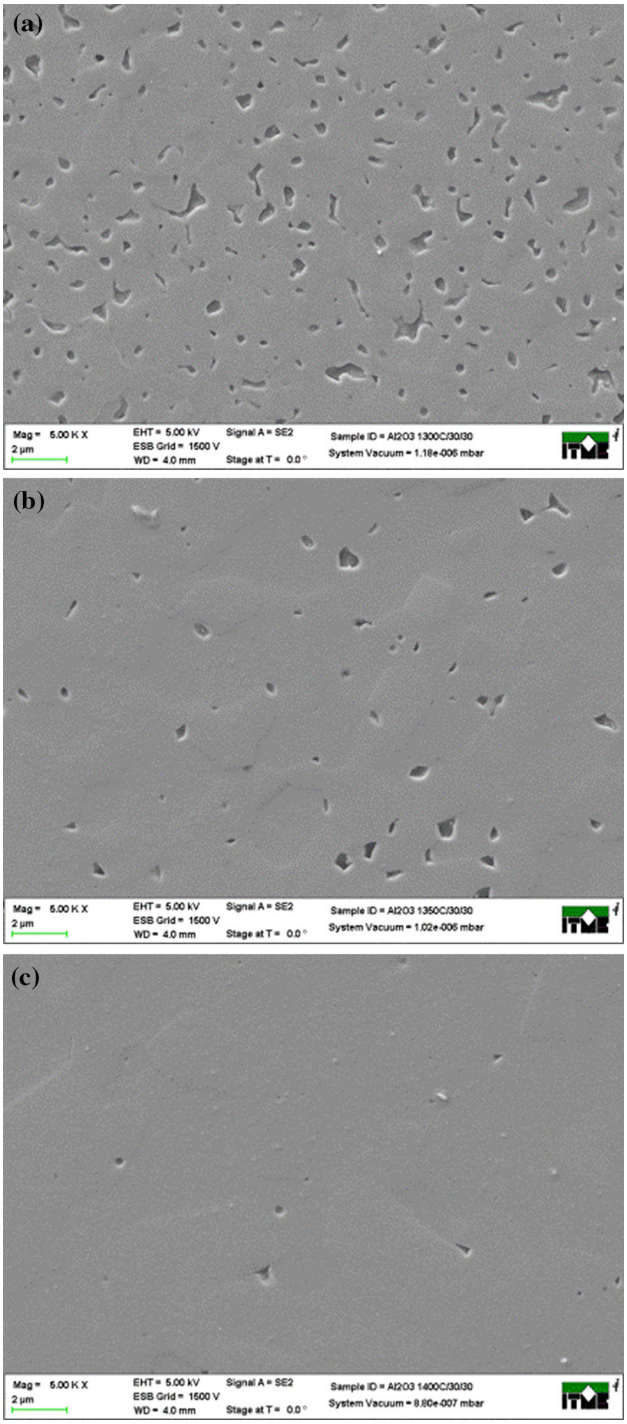

Fig. 4 SEM images of sintered aluminum oxide at different conditions: (a) T_s = 1300 °C, t_s = 30 min, p = 30 MPa, (b) T_s = 1350 °C, t_s = 30 min, p = 30 MPa, (c) T_s = 1400 °C, t_s = 30 min, p = 30 MPa

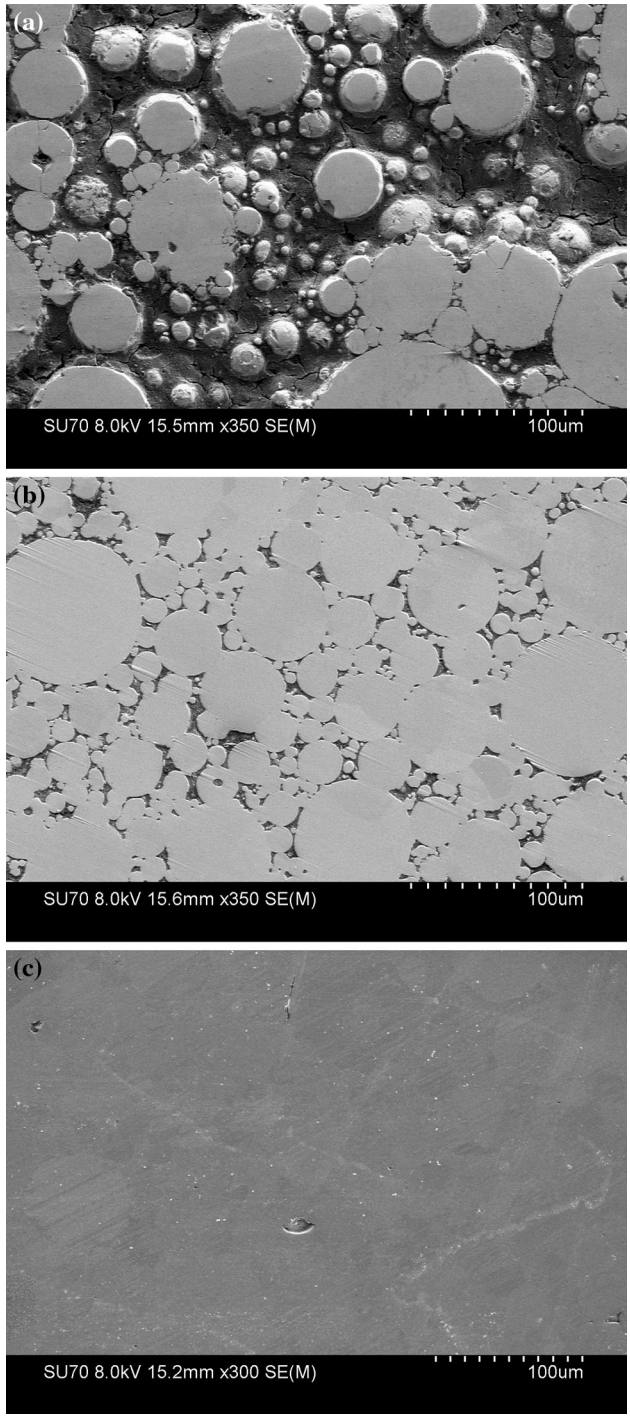

Fig. 5 SEM images of sintered NiAl material at different conditions: (a) T_s = 1300 °C, t_s = 10 min, p = 5 MPa, (b) T_s = 1400 °C, t_s = 10 min, p = 5 MPa, (c) T_s = 1400 °C, t_s = 30 min, p = 30 MPa

correlated with the sintering temperature. Depending on the sintering temperature, different mass transport mechanisms (surface diffusion, evaporation-condensation, grain boundary diffusion, viscous flow, volume diffusion) are dominant, e.g., surface diffusion dominates the low-temperature sintering. Based on Fig. 2. it can be concluded that densification is improved with the rise of temperature for all types of sintered materials.

3.2 Microstructure Investigations

3.2.1 Sintered Al_2O_3 Ceramics. Depending on the type, chemical composition, and required properties, the elements based on sintered aluminum oxide can be sintered under different technological conditions and, most importantly, at a wide temperature range, i.e., between 1400 and 1900 °C (Ref 27). An essential prerequisite for the initiation of the sintering process of loose powders is their packing in a manner enabling both their

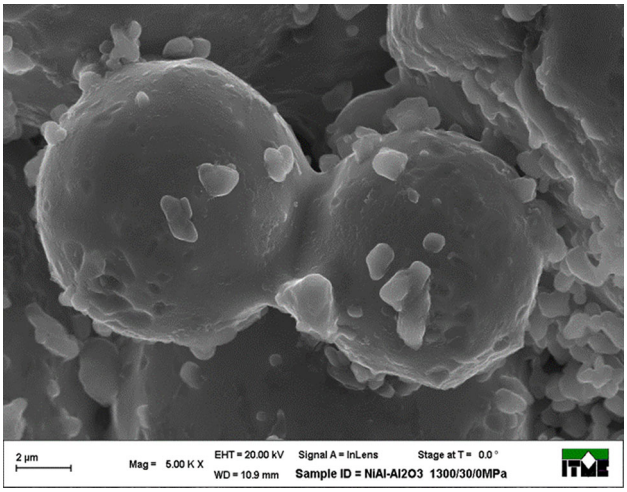

Fig. 6 SEM images of sintered NiAl/Al_2O_3 material at early stage of sintering process: (a) T_s = 1300 °C, t_s = 30 min, p = 5 MPa

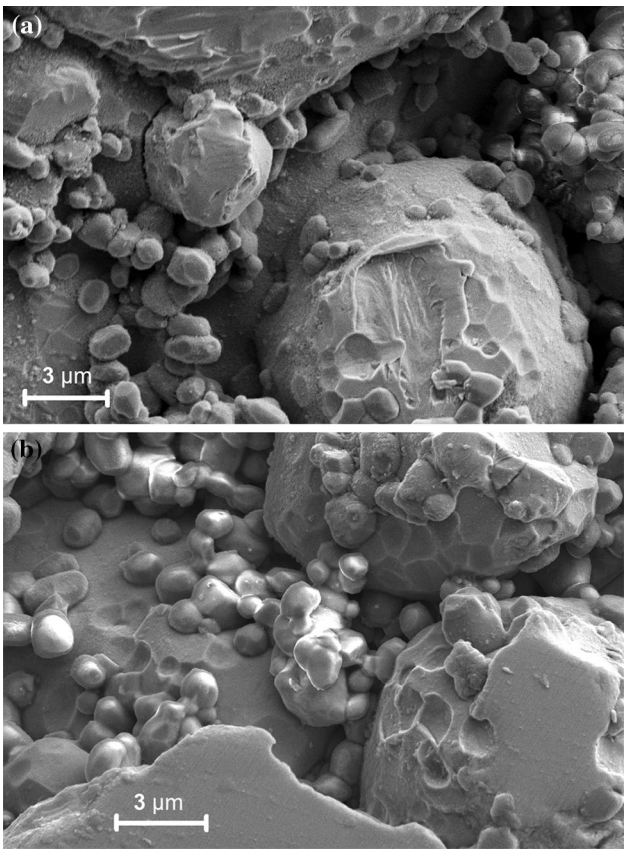

Fig. 7 Intermediate stage of NiAl-Al_2O_3 composite material sintering: (a) T_s = 1350 °C, t_s = 30 min, p = 5 MPa, (b) T_s = 1400 °C, t_s = 30 min, p = 5 MPa

interaction and the arrangement's reaching the temperature at which the atomic activity was sufficient to start the process. At the initial stage of Al_2O_3 sintering, intergranular contacts are created, which is a precondition for the transport of the mass between grains. Contacts with the biggest surface areas possible are formed through a proper dispergation of the sintered powders or the application of external force. The concentration gradient of lattice vacancies at the contact points of grains and, more

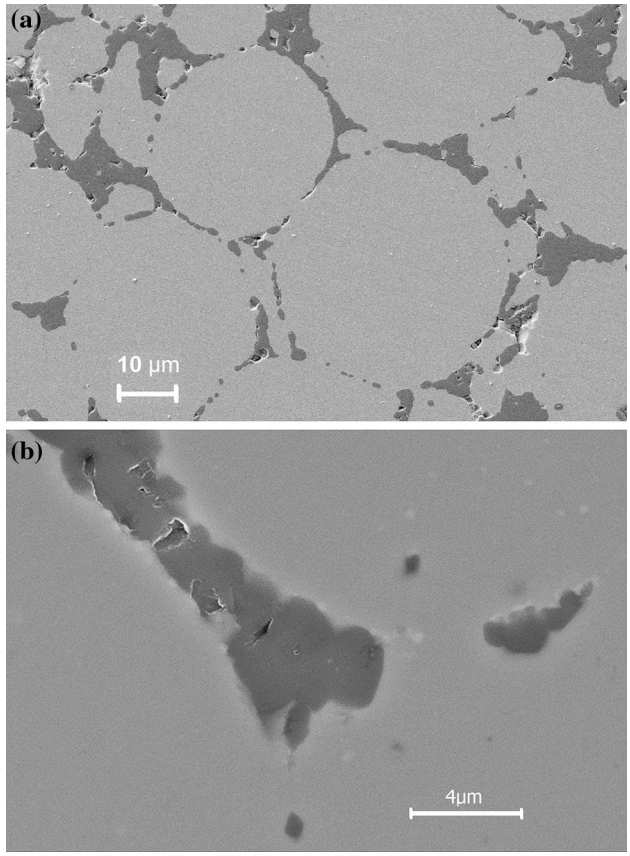

Fig. 8 SEM images of sintered NiAl/Al_2O_3 material at final stage of sintering process (T_s = 1400 °C, t_s = 30 min, p = 30 MPa)

specifically, between the free grain surface and the contact surface, i.e., the nucleus of the future neck, is the driving force of the sintering process. This can be observed in Fig. 3a. The intermediate phase of aluminum oxide's sintering begins with the changes in grain boundaries and the size of pores which are targeted at taking cylindrical shapes. This stage ends once pore shrinkage has taken place (Fig. 3b).

There are two alternative final stages of sintering which begins with a significant reduction of the pore volume. The first one takes place under conditions enabling pores to eventually locate in the corners of three or four grains (Fig. 4), whereas the second one occurs when a fast discontinuous growth of grains precedes the movements of pores aimed at finding energetically suitable areas and closing them inside crystallites (Ref 28). This phenomenon was not observed in the studied case.

Any geometrical changes in the shape and dimensions of aluminum oxide grains are a result of diffusive processes. On the other hand, diffusive transfer of ions is directly related to the movement of vacancies which are agglomerated on the pore surface move toward grain boundaries and subsequently migrate toward them. As a result of these changes, the material with a negligible number of pores is eventually thickened.

3.2.2 Sintered NiAl Material. During the sintering process, NiAl particulate is converted into a polycrystalline material. The evolution of microstructure during sintering is shown in Fig. 5. At the initial stage, (Fig. 5a) cohesive bonds are formed between particles. When the sintering process is continued (Fig. 5b), the necks between particles grow due to the mass transport. The surface and grain boundary diffusion

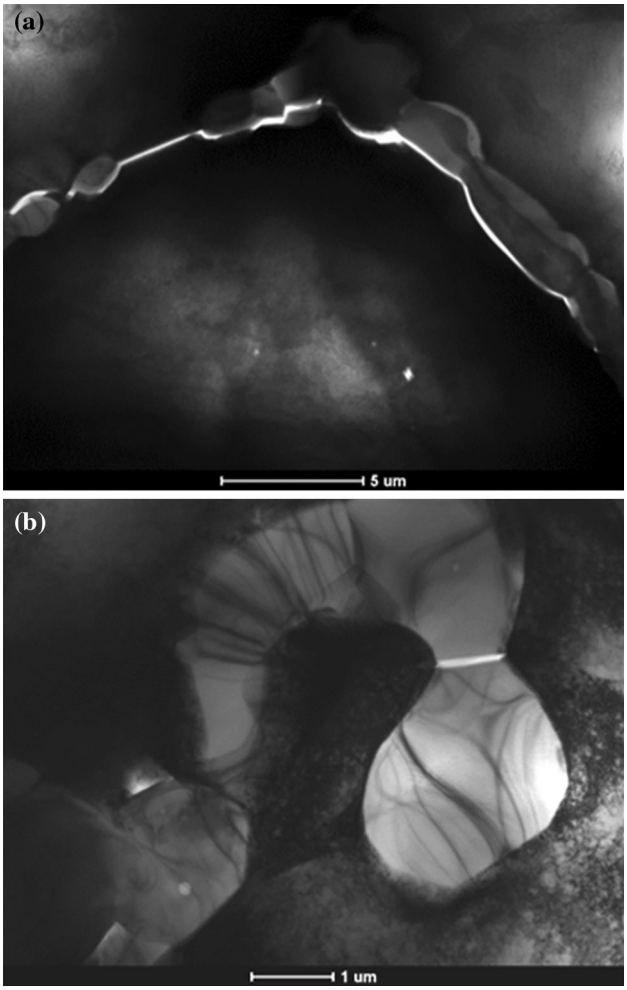

Fig. 9 TEM micrographs of $NiAl/Al_2O_3$ composites: (a) T_s = 1350 °C, t_s = 30 min, p = 30 MPa, (b) T_s = 1400 °C, t_s = 30 min, p = 30 MPa

are usually dominant mass transport mechanisms in case of sintering (Ref 1). As a result of the stresses in the neck and the surface tension, the particles are attracted to each other, which leads to the shrinkage of the system. The described processes, shrinkage, and mass transport are inextricably linked to the total reduction of material porosity (Fig. 5c).

3.2.3 Sintered NiAl-Al_2O_3 Composite. The formation of adhesive contacts between particular grains should be treated as a starting point of the sintering process of composite materials. Subjecting the system of particles to temperature results in the appearance of intergranular necks (Fig. 6). It was observed that the necks were formed between grains of the same material (NiAl-NiAl and Al_2O_3-Al_2O_3) as well as between metallic phase particles and aluminum oxide grains. At first, the necks were relatively small with low durability; however, with time, they enlarged and the material gradually became thicker. Smaller aluminum oxide grains either occurred in the form of single grains on the surface of NiAl grains or formed bigger systems in the area where few NiAl grains were in contact.

The intermediate stage of sintering is characterized by simultaneous pore rounding, densification as well as grain growth and is controlled by the diffusion processes. As seen in Fig. 7a, when increasing temperature, the necks begin to grow and a more compact structure is formed. Bonded grains can be observed in systems consisting of more than two grains. The average distance between adjacent grains decreases and the size of necks grows. Ceramic grains are also connected with each other. The rise in temperature to 1400 °C results in the sintering of Al_2O_3 particles (Fig. 7b).

The final stage of the $NiAl/Al_2O_3$ sintering process is characterized by elimination of pores in the composite structure. When compared to the initial and intermediate stages, the final-stage sintering is a relatively slow process. A complex interaction between particles, pores and grain boundaries plays a crucial role in the final densification. As seen in Fig. 8b, some tiny pores can be trapped between ceramic particles. Such structural defects, especially at the $NiAl/Al_2O_3$ interface, can affect the mechanical properties of materials.

The presented analysis of the microstructure proves that the choice of technological conditions of sintering determines the progress in the material's thickening process and, at the same time, its properties. Through the control of the temperature, time, and pressure of the sintering process, it is possible to obtain a material with an acceptable level of porosity which in turn can be almost entirely eliminated.

SEM observations of fracture surfaces indicate brittle character of cracking; however, the path of cracking is different for pure NiAl and composite material. Failure in the pure NiAl phase runs characteristically in one direction through the NiAl grains, whereas the ceramic grains force the crack to wind its way across the ceramic material, which greatly elongates its path and thereby increases the strength of the composite. As a result, the bending strength of composite materials is also raised (Ref 19).

3.2.4 TEM Studies of Ceramic-Metal Interface. In case of multiphase materials, the interface plays a decisive role. The properties of the designed materials will mainly depend on the quality of the said coupling. Properly selected sintering conditions should render the formation of a permanent coupling between a composite's components through its entire volume attainable. Couplings between ceramic grains and NiAl were created in case of sintering performed at 1300 °C. Nevertheless, at first they were observable only at some points. With the increase in the sintering temperature, the process progressed until the composite's components was fully and permanently bound. Figure 9 depicts an exemplary NiAl-Al_2O_3 interface for selected sintering conditions.

Figure 9 shows transmission electron micrographs in which Al_2O_3 can be seen when the contrast is brighter, while NiAl is observable when the contrast is darker due to the orientation's being close to symmetrical and a relatively high density of dislocations. The ceramic phase is located at NiAl grain boundaries. The interface is relatively clean with no additional phases that could have been formed during the sintering process. It indicates a good quality of the sintered samples, since the formation of the transition phase resulting from the reaction between both phases would have weakened the interface.

Similar observations can be made based on Fig. 10 at a slightly higher magnification. Moreover, a high density of dislocations can be seen in the NiAl phase. A few stacking faults are observed in Al_2O_3. There is no crystallographic relation between both phases. The orientation relationships are rather random. Diffraction pattern is only useful for identifying the phases. It was confirmed in the microanalysis performed using a TEM EDS detector that along the marked line across

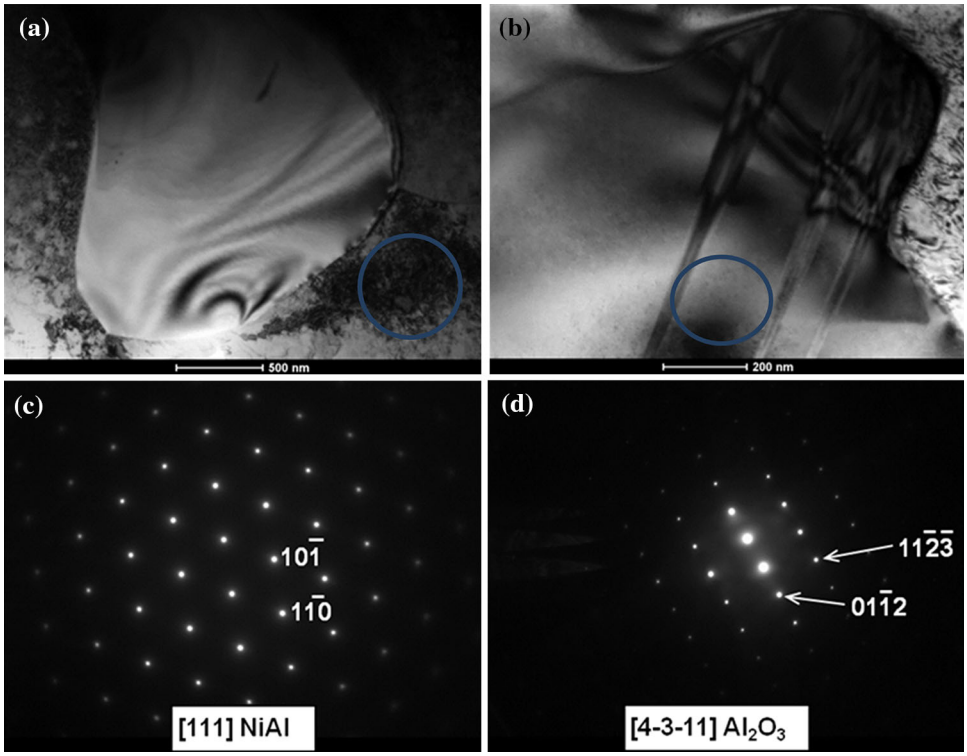

Fig. 10 TEM micrographs of NiAl/Al_2O_3 composites (a, b) and (c) selected area diffraction pattern (SADP) from the area marked by a circle in (a) and (d) SADP from the area marked by a circle in (b) The zone axis resulting from the distances and angles between reflections in SADPs is indicated

the interface there were changes in the content of Ni, O, and Al, which did not indicate the presence of any transition phases (Fig. 11). The TEM analyses proved that the bond at the NiAl/Al_2O_3 interface was quite strong and had an adhesive character. The contrast change at the interface also suggested that no diffusive type interface layer was formed.

3.3 Elastic Properties

The elastic constants of the obtained sintered samples were determined based on the measurements of ultrasonic velocities described in section 2. Table 4 presents detailed results of measurements of the Young's modulus E and Poisson's ratio v for pure ceramic Al_2O_3, pure intermetallic NiAl, and NiAl/Al_2O_3 composite samples sintered in different conditions. Based on the presented values, the relations between elastic moduli and the relative density ρ_{rel} for three considered materials are illustrated in Fig. 12. In all cases, the substantial increase of the Young's modulus with the relative density can be seen. For example, for pure ceramics, the difference between the maximum and minimum value of E equals 78%. The change of the Poisson's ratio is less pronounced. Only in case of NiAl material a slight increase of Poisson's ratio can be observed with the increase in density. The growth of the Young's modulus of Al_2O_3 and NiAl during the material's densification is similar. Additionally, in case of the Poisson's ratio, its growth for the intermetallic material is more significant than for ceramics.

The values of elastic constants of the NiAl/Al_2O_3 composite apparently depend on the values of elastic constants of its constituent phases with respect to the volume content. Due to the intermetallic and ceramic phase content in the analyzed composite material, i.e., 80% of NiAl and 20% of Al_2O_3, the value of NiAl/Al_2O_3 elastic constants should be close to the intermetallic one. Particularly at low relative density, $\rho_{rel} < 0.95$, this trend is confirmed regardless of the sintering parameters—the results of the composite's Young's modulus are fairly similar to the Young's modulus of NiAl (Fig. 12a).

The explanation of this homogeneity of results can be found in the section devoted to the microstructure. Figure 13(a) and (b) shows the microstructure of NiAl/Al_2O_3 and NiAl samples with relative density close to 0.9. In the first one, we can see a skeleton with small alumina particles created on the surface of NiAl grains. At low densities, these small ceramic grains located on the NiAl surface have no impact on the stiffness of the composite. In comparison to pure NiAl samples, ceramic particles in composite materials slightly reduce the porosity with no significant effect on the stiffness. For higher relative densities, $\rho_{rel} > 0.95$, ceramic particles are strongly connected with intermetallic ones in the whole volume of the composite material (Fig. 8), which is the major reason for a higher stiffness than in case of pure intermetallic material.

The value of elastic constants for fully dense composite can be calculated theoretically from well-known models, such as Voigt-Reuss, or Hashin-Shtrikman limits (Ref 22, 23). From the values of elasticity moduli measured on fully dense specimens of pure NiAl and Al_2O_3 (see Table 4), one can calculate the theoretical limits for Young's modulus of the NiAl/Al_2O_3 composite. They are, Voigt-Reuss: 202.5—227.7 GPa and Hashin-Shtrikman: 212.6—217.0 GPa, respectively. The maximum value measured on the samples of NiAl/Al_2O_3 composite—219 GPa is well within Voigt-Reuss limits but slightly

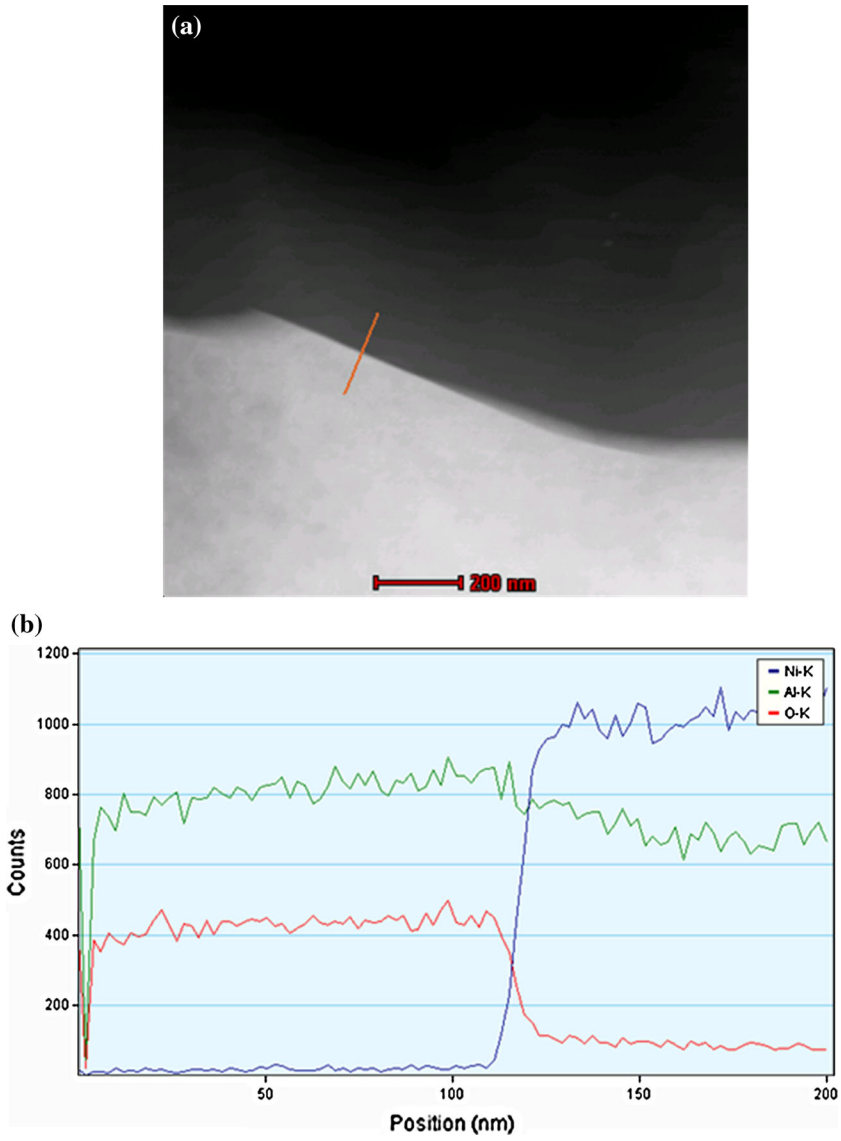

Fig. 11 Scanning transmission electron micrograph (a) and changes of the content of Al, O, Ni along the marked line (b)

above the Hashin-Shtrikman limits. This minor discrepancy may be caused by measurement errors as well as by some statistical fluctuations in the real phase content of the NiAl/Al_2O_3 specimens.

The influence of the sintering temperature T_s, sintering time t_s, and external pressure p on the elastic properties of the ceramic, intermetallic, and composite samples is well-illustrated in Fig. 14(a) and (c), respectively. It is rather obvious that for all three materials the elastic modulus rose when increasing all three sintering parameters. It can be seen that samples manufactured at theoretically least favorable sintering conditions show low and dissatisfactory values of material stiffness. Specifically the ceramic materials require better sintering parameters to avoid a situation where the Young's modulus for the samples stays at the level of 22% of the Young's modulus for fully dense alumina E_0 (T_s = 1300 °C, t_s = 0 min, p = 5 MPa). In general, all materials sintered at low pressure (5 MPa) have a very low Young's modulus, regardless of other sintering parameters (temperature and time). Obviously, the main reason for such low stiffness is insufficient material densification; however, the effect of the microstructure's features should also be considered. Figure 3 and 7 presents the microstructure of both ceramic and composite samples with a low value of E, where high distribution of irregularly shaped pores can be observed. Sintered materials exhibit a decreasing strength (and stiffness) when the pore shape becomes irregular; small spherical pores are preferable. Creating favorable pore configuration depends on the process conditions (Ref 1). Furthermore, it should be stated that, because of the low relative density of materials (in the presence of the second phase higher density is not possible to obtain under these conditions), the stiffness of composite specimens sintered at 5 MPa is lower than for NiAl sintered under the same conditions (9 examples). Based on the results of TEM investigations (section 3.2.4), one can observe that the addition of the ceramic phase is linked with the occurrence of an adhesive contact between intermetallic and alumina particles. The quality of the NiAl-Al_2O_3 bond depends on the applied

Table 4 Evolution of elastic mechanical properties of hot-pressed Al_2O_3, NiAl, and NiAl/Al_2O_3 samples determined by ultrasonic measurements

sintering process parameters			Al_2O_3		NiAl		NiAl/Al_2O_3	
T_s (°C)	t_s (min)	p (MPa)	Young's modulus E (GPa)	Poisson's ratio ν	Young's modulus E (GPa)	Poisson's ratio ν	Young's modulus E (GPa)	Poisson's ratio ν
1300	0	5	88	0.221	70	0.283	44	0.258
1350	0	5	136	0.221	81	0.288	53	0.242
1400	0	5	238	0.217	127	0.289	56	0.268
1300	10	5	130	0.218	82	0.286	61	0.275
1350	10	5	197	0.219	116	0.282	81	0.277
1400	10	5	235	0.220	135	0.286	85	0.277
1300	30	5	195	0.217	88	0.279	67	0.280
1350	30	5	242	0.230	131	0.291	81	0.259
1400	30	5	323	0.220	149	0.296	117	0.271
1300	0	30	238	0.212	122	0.301	151	0.294
1350	0	30	303	0.227	134	0.297	175	0.292
1400	0	30	397	0.227	153	0.305	195	0.292
1300	10	30	307	0.225	157	0.313	164	0.284
1350	10	30	382	0.231	169	0.307	186	0.291
1400	10	30	400	0.222	176	0.313	208	0.297
1300	30	30	357	0.231	167	0.309	214	0.285
1350	30	30	393	0.230	178	0.313	218	0.287
1400	30	30	404	0.232	183	0.318	219	0.286

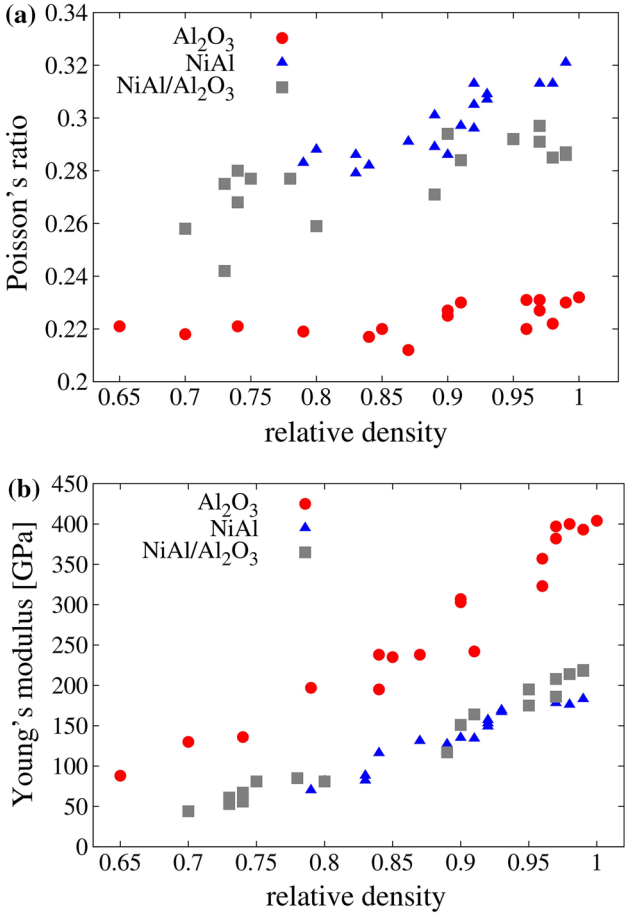

Fig. 12 Experimental results of: (a) Young's modulus, and (b) Poisson's ratio of hot-pressed Al_2O_3, NiAl, and NiAl/Al_2O_3 samples as a function of relative density

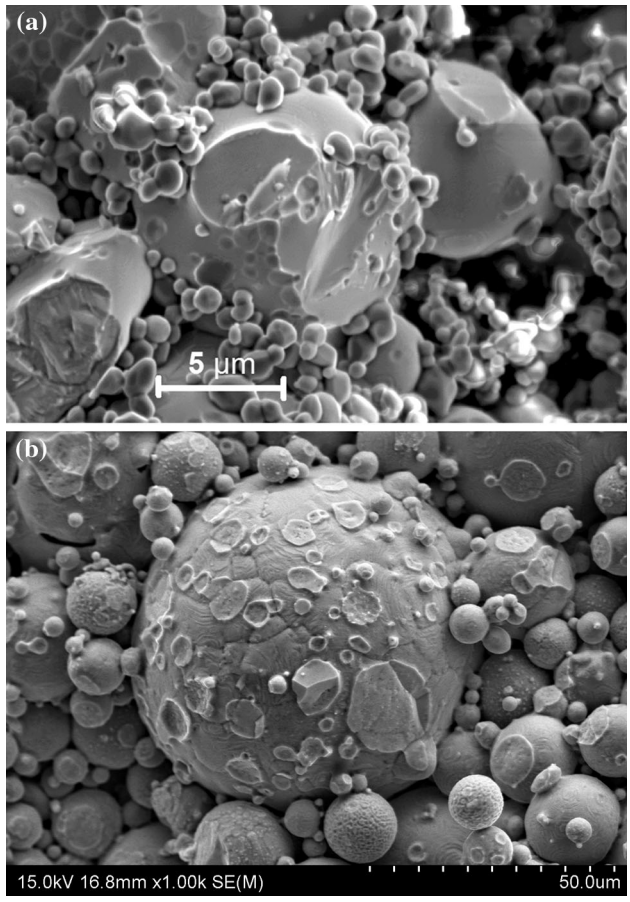

Fig. 13 Comparison of the microstructure of: (a) NiAl-Al_2O_3, and (b) NiAl samples at the approximate stage of densification (ρ_{rel} 0.90)

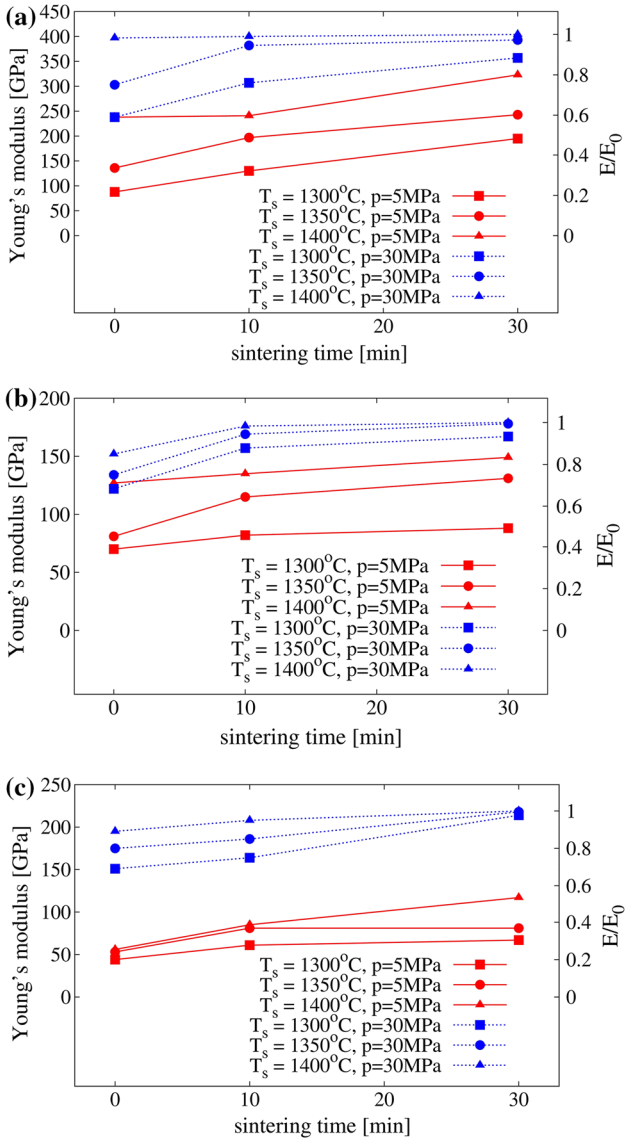

Fig. 14 Experimental results of Young's modulus of: (a) pure Al_2O_3, (b) pure NiAl, and c) $NiAl/Al_2O_3$ samples manufactured at a different combinations of sintering temperatures and pressures as a function of the sintering time (E_0—the Young's modulus of a fully dense material)

pressure. The importance of sintering pressure as a critical parameter in the manufacturing process can be particularly seen in the case of a composite material for which the difference between the Young's modulus for the samples sintered at 5 and 30 MPa is the most significant (Fig. 14c). The application of higher external pressure (30 MPa) intensifies the penetration of the intermetallic and ceramic particles, at the same time allowing us to obtain a material with a low-porosity structure and a low number of isolated spherical pores (Fig. 8). Generally, samples manufactured at higher pressure are characterized by the Young's modulus between 87 and 100% of the value for fully dense samples.

4. Conclusions

In the present work, a comparison was made between the sinterability of a two-phase $NiAl-Al_2O_3$ composite material and the sinterability of its separate components as a function of the parameters of the sintering process (temperature, time, and pressure). The proper choice of these parameters enables for obtaining materials characterized by density close to the theoretical one. The observation of the structure of the sintered materials rendered the determination of particular sintering stages possible for both single-phase and compound materials. It was discovered that the formation of couplings between concrete composite components (i.e., NiAl-NiAl, $Al_2O_3-Al_2O_3$, and $NiAl-Al_2O_3$) took place at about the same sintering time and the quality (the Young's modulus) of these couplings improved as the sintering process progressed. The examination of the matrix-reinforcement interface proved the existence of a strong adhesive coupling. No new phases were found at the ceramics-metal phase boundary.

The values of elastic constants of $NiAl/Al_2O_3$ were close to intermetallic ones due to the volume content of the NiAl phase. The Young's modulus and the Poisson's ratio of the analyzed composite material was similar to these in case of NiAl, especially at low densities, in case of which small alumina particles had no impact on the composite's stiffness. The influence of external pressure of 30 MPa seemed crucial for obtaining a satisfactory stiffness for three kinds of the studied materials, which were characterized by a high dense microstructure with a low number of isolated spherical pores.

Based on the sintering tests performed for particular composite components, preliminary information on the properties of two-phase materials was collected, which is likely to have a tremendous influence on the design of new materials with required characteristics.

Acknowledgment

The results presented in this paper have been obtained within the projects funded by the National Science Centre awarded by decisions number DEC-2012/05/N/ST8/03376 and DEC-2013/11/B/ST8/03287, Operational Programme Human Capital 8.2.1 "Wsparcie przedsiębiorczości naukowców bio tech med poprzez stypendia, staże i szkolenia," as well as "KomCerMet" project (contract no. POIG.01.03.01-14-013/08-00 with the Polish Ministry of Science and Higher Education) within the framework of the Operational Programme Innovative Economy 2007-2013.

Open Access

This article is distributed under the terms of the Creative Commons Attribution License which permits any use, distribution, and reproduction in any medium, provided the original author(s) and the source are credited.

References

1. R.M. German, *Sintering—Theory and Practice*, A Wiley Interscience Publications, New York, 1996
2. P. Nieroda, R. Zybala, and K.T. Wojciechowski, Development of the method for the preparation of Mg2Si by SPS technique, *Am. Inst. Phys. Conf. Proc.*, 2012, **1449**, p 199–202
3. M. Chmielewski and K. Pietrzak, Processing, Microstructure and Mechanical Properties of Al_2O_3-Cr Nanocomposites, *J. Eur. Ceram. Soc.*, 2007, **27**, p 1273–1279
4. W. Olesińska, D. Kaliński, M. Chmielewski, R. Diduszko, and W. Włosiński, Influence of Titanium on the Formation of a "Barrier"

Layer During Joining an AlN Ceramic with Copper by the CDB Technique, *J. Mater. Sci.: Mater. Electron.*, 2006, **17**, p 781–788
5. M. Barlak, J. Piekoszewski, J. Stanislawski, Z. Werner, K. Borkowska, M. Chmielewski, B. Sartowska, M. Miskiewicz, W. Starosta, L. Walis, and J. Jagielski, The Effect of Intense Plasma Pulse Pre-Treatment on Wettability in Ceramic-Copper System, *Fusion Eng. Des.*, 2007, **82**, p 2524–2530
6. K. Pietrzak, D. Kaliński, and M. Chmielewski, Interlayer of Al_2O_3-Cr Functionally Graded Material for Reduction of Thermal Stresses in Alumina—Heat Resisting Steel Joints, *J. Eur. Ceram. Soc.*, 2007, **27**(2-3), p 1281–1286
7. W. Włosiński and T. Chmielewski, Plasma-Hardfaced Chromium Protective Coatings-Effect of Ceramic Reinforcement on Their Wettability by Glass, *Adv. Sci. Technol.*, 2003, **32**, p 253–260
8. K. Wojciechowski, R. Zybala, and R. Mania, High Temperature CoSb3—Cu Junctions, *Microelectron. Reliab.*, 2011, **51**, p 1198–1202
9. M. Barlak, W. Olesińska, J. Piekoszewski, Z. Werner, M. Chmielewski, J. Jagielski, D. Kaliński, B. Sartowska, and K. Borkowska, Ion Beam Modification of Ceramic Component Prior to Formation of AlN-Cu Joints by Direct Bonding Process, *Surf. Coat. Technol.*, 2007, **201**, p 8317–8321
10. T. Zhang, H. Guo, S. Gong, and H. Xu, Effects of Dy on the Adherence of Al_2O_3/NiAl Interface: A Combined First-Principles and Experimental Studies, *Corrosion Sci.*, 2013, **66**, p 59–66
11. K. Morsi, Review: Reaction Synthesis Processing of Ni-Al Intermetallic Materials, *Mater. Sci. Eng. A*, 2001, **299**, p 1–15
12. R. Darolia, Ductility and Fracture Toughness Issues Related to Implementation of NiAl for Gas Turbine Applications, *Intermetallics*, 2000, **8**, p 1321–1327
13. T. Chmielewski and D.A. Golański, New Method of In-Situ Fabrication of Protective Coatings Based on Fe-Al Intermetallic Compounds, *Proc. Inst. Mech. Eng. Part B*, 2011, **225**(B4), p 611–616
14. K. Matsuura, T. Kitamutra, and M. Kudoh, Microstructure and Mechanical Properties of NiAl Intermetallic Compound Synthesized by Reactive Sintering Under Pressure, *J. Mater. Process. Technol.*, 1997, **63**, p 293–302
15. D. Tingaud and F. Nardou, Influence of Non-Reactive Particles on the Microstructure of NiAl and NiAl-ZrO_2 Process by Thermal Explosion, *Intermetallics*, 2008, **16**, p 732–737
16. J. Cook, C.C. Evans, J.E. Gordon, and D.M. Marsh, Mechanism for Control of Crack Propagation in All-Brittle Systems, *Proc. R. Soc. Lond. Ser. A*, 1964, **282**(1390), p 508–520
17. W.H. Tuan, Toughening Alumina with Nickel Aluminide Inclusions, *J. Eur. Ceram. Soc.*, 2000, **20**, p 895–899
18. W.H. Tuan, W.B. Chou, H.C. You, and S.T. Chang, The Effects of Microstructure on the Mechanical Properties of $A1_2O_3$-NiAl Composites, *Mater. Chem. Phys.*, 1998, **56**, p 157–162
19. D. Kaliński, M. Chmielewski, and K. Pietrzak, An Influence of Mechanical Mixing and Hot-Pressing on Properties of NiAl/Al_2O_3 Composite, *Arch. Metall. Mater.*, 2012, **57**(3), p 694–702
20. M. Chmielewski, D. Kaliński, K. Pietrzak, and W. Włosiński, Relationship Between Mixing Conditions and Properties of Sintered 20AlN/80Cu Composite Materials, *Arch. Metall. Mater.*, 2010, **55**(2), p 579–585
21. C.L. Hsieh, W.H. Tuan, and T.T. Wu, Elastic Behaviour of a Model Two-phase material, *J. Eur. Ceram. Soc.*, 2004, **24**, p 3789–3793
22. C.L. Hsieh and W.H. Tuan, Elastic Properties of Ceramic Metal Particulate Composites, *Mater. Sci. Eng. A*, 2005, **393**, p 133–139
23. H.A. Bruck, Y.M. Shabana, B. Xu, and J. Laskis, Evolution of Elastic Mechanical Properties During Pressureless Sintering of Powder-Processed Metals and Ceramics, *J. Mater. Sci.*, 2007, **42**, p 7708–7715
24. S. Nosewicz, J. Rojek, S. Mackiewicz, M. Chmielewski, K. Pietrzak, and B. Romelczyk, The Influence of Hot Pressing Conditions on Mechanical Properties of Nickel Aluminide/Alumina Composite, *J. Compos. Mater.*, 2014, (In press), doi: 10.1177/0021998313511652
25. L. Nicolas and A. Borzacchiello, *Encyclopedia of Composites*, 2nd ed., Wiley, New Jersey, 2012
26. J. Bidulská, R. Bidulský, T. Kvačkaj, and M.A. Grande, Porosity Evolution in Relation to Microstructure /Fracture of ECAPed PM Al-Mg-Si-Cu-Fe Alloy, *Steel Res Int*, SI, 2012, p 1191-1194
27. E.K.H. Li and P.D. Funkenbusch, Hot Isostatic Pressing (HIP) of Powder Mixtures and Composites, *Metall. Trans.*, 1993, **24A**, p 1345–1354
28. J. Lis and R. Pampuch, The Role of Surface-Diffusion in the Sintering of Micropowders, *J. Phys.*, 1986, **47**, p 219–223